Damage extraction of buildings in the 2015 Gorkha, Nepal earthquake from high-resolution SAR data

Fumio Yamazaki*[a], Rendy Bahri[a], Wen Liu[a], Tadashi Sasagawa[b]
[a]Graduate School of Eng., Chiba University, 1-33 Yayoi-cho, Inage-ku, Chiba, Japan 263-8522;
[b]PASCO Co., 4-10-1 Nakano, Nakano-ku, Tokyo, Japan 164-0001

ABSTRACT

Satellite remote sensing is recognized as one of the effective tools for detecting and monitoring affected areas due to natural disasters. Since SAR sensors can capture images not only at daytime but also at nighttime and under cloud-cover conditions, they are especially useful at an emergency response period. In this study, multi-temporal high-resolution TerraSAR-X images were used for damage inspection of the Kathmandu area, which was severely affected by the April 25, 2015 Gorkha Earthquake. The SAR images obtained before and after the earthquake were utilized for calculating the difference and correlation coefficient of backscatter. The affected areas were identified by high values of the absolute difference and low values of the correlation coefficient. The post-event high-resolution optical satellite images were employed as ground truth data to verify our results. Although it was difficult to estimate the damage levels for individual buildings, the high resolution SAR images could illustrate their capability in detecting collapsed buildings at emergency response times.

Keywords: The 2015 Nepal earthquake, TerraSAR-X, building damage, change detection

1. INTRODUCTION

An Mw7.8 earthquake hit Nepal at 11: 56 AM (local time, 06:11UTC) on April 25, 2013. The epicenter was located at 28. 23° N, 84.73° E, with a shallow focal depth of 8 km. This earthquake was caused by thrust faulting between the subducting India Plate and the overriding Eurasia Plate. According to the fault model calculated from seismic waveforms by USGS [1], the causative fault plane is 20 km in length and 15 km in width with 295-degrees strike angle and 10-degrees dip angle. Due to the strong motion in a wide area, it became the worst natural disaster in Nepal since the 1934 Bihar, Nepal earthquake. More than 8,600 people were killed in Nepal and 161 people in the surrounding countries due to building collapses, landslides and avalanches triggered by the strong shaking [2]. Thousands of houses were destroyed and more than 450,000 people were displaced. Several famous monuments, such as pagodas in Kathmandu Durbar Square and Dharahara tower, were collapsed and many tourists were killed. Since the Tribhuvan International Airport was closed immediately after the earthquake and a number of roads were blocked by landslides, international aid activities and field reconnaissance surveys were difficult to carry out for a few days.

Remote sensing is recognized as an effective tool for detecting and monitoring the affected areas due to natural disasters. There are mainly two categories of remote sensing from the sensor type: the passive remote sensing (mainly optical sensors) and the active remote sensing (mainly radar sensors). Optical satellite system only works in the daytime and cannot observe objects under cloud-cover conditions. However, a radar system as Synthetic Aperture Radar (SAR) overcomes this problem. Due to remarkable improvements in radar sensors, high-resolution TerraSAR-X, COSMO-SkyMed, and PALSAR-2 images are available with ground resolution of 1 to 5 m, providing detailed surface information.

A number of researches have been carried out on rapid damage assessment after natural disasters using SAR data. Interferometric analysis is one of the most powerful methods to detect crustal movements and also to investigate building damages [3, 4]. Matsuoka and Yamazaki [5] performed a feasibility study on the backscattering characteristics of damaged areas in the 1995 Kobe, Japan earthquake, and developed an automated method to detect hard-hit areas using ERS SAR intensity images. The method was also applied to Envisat ASAR images in the 2003 Bam, Iran earthquake [6]. Recently, several studies attempted to detect damage at the scale of a single building unit, using both high-resolution optical and SAR images [7-10].

* fumio.yamazaki@faculty.chiba-u.jp; phone +81-43-290-3557; fax +81-43-290-3558.

Land Surface and Cryosphere Remote Sensing III, edited by Reza Khanbilvardi, Ashwagosh Ganju, A. S. Rajawat, Jing M. Chen, Proc. of SPIE Vol. 9877, 98772K · © 2016 SPIE
CCC code: 0277-786X/16/$18 · doi: 10.1117/12.2223306

In this study, pre- and post-event TerraSAR-X images are used to estimate building damage in Kathmandu caused by the 2015 Nepal earthquake. The difference and correlation coefficient of the backscattering coefficients at two time instants are used to identify collapsed buildings. Comparing with pre- and post-event high-resolution optical satellite images and field survey reports, the accuracy of damage extraction from the high-resolution SAR data is evaluated.

2. STUDY AREA AND IMAGE DATA

This study focuses on the capital city, Kathmandu. The location of the fault plane and the epicenter determined by USGS are shown in Figure 1(a) by the blue shade and the star mark [1]. Kathmandu is located just above the south edge of the causative fault-plane and the estimated MM intensity was in the range of VI to IX. The population in Kathmandu was about 1.7 million before the event, and 1,203 people were killed and 4,634 injured [2]. Since mass media broadcasted the situation of severely damaged buildings repeatedly, including historical monuments in the Kathmandu Valley, the capital city was thought completely reduced to ruin. But the Japanese investigation team reported that the most parts of the city were in rather minor damage situation [11].

One pre-event and one post-event TerraSAR-X (TSX) imagery data were used in this study. The pre-event image was taken on October 13, 2013 (12:19:03 UTC) whereas the post-event image was taken on April 27, 2015 (12:19:03 UTC), two days after the mainshock. The observation conditions of the two data were almost the same, the incident angle 39.5° at the center of the images, from the ascending path with a heading of 350° clockwise from the north. The data were captured with the VV polarization in the SpotLight (SL) mode, provided by the Single-look Slant-range Complex (SSC) product [12]. The resolution was 1.6 m in the azimuth and 1.85 m in the ground range directions, and the georeferenced intensity data were resampled with the pixel size of 1.5 m. An Enhanced Lee filter (3x3) was applied to the original SAR images to reduce the speckle noise. Radiometric calibration was then carried out to get the backscattering coefficient (sigma naught, σ^0) in the ground range in the decibel (dB) unit. The color-composite of the obtained pre- and post-event images is shown in Figure 1(b), in which the study area was selected within a yellow square in the central Katmandu.

Pre-event and post-event high-resolution optical satellite images were also introduced as the truth data of building damage in the study area. The pre-event WorldView-3 (WV3) image was acquired on October 25, 2014 (04:59:37 UTC) with off-nadir angle 21°, and the post-event GeoEye-1 (GE1) image on May 3, 2015 (04:59:26 UTC) with off-nadir angle 23°. For the two temporal images, the bundle products of the panchromatic (Pan) and four multi-spectral (BGR and near-IR) bands were introduced. After a pansharpening process, the pre-event WV3 image has the spatial resolution of 30 cm and the post-event GE1 image 50 cm. Figure 2 depicts the enlarged SAR and optical images for the study area.

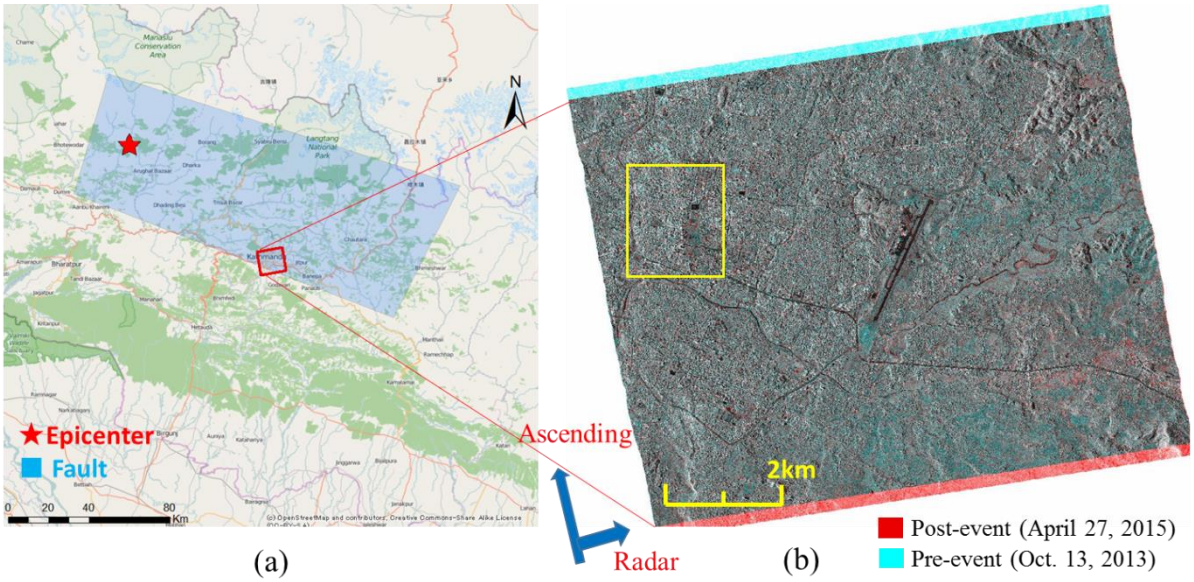

Figure 1. Locations of the epicenter and fault plane of the Gorkha earthquake (a) and the color composite of the pre- and post-event TerraSAR-X images of the central Kathmandu area (b). The yellow square shows the detailed study area.

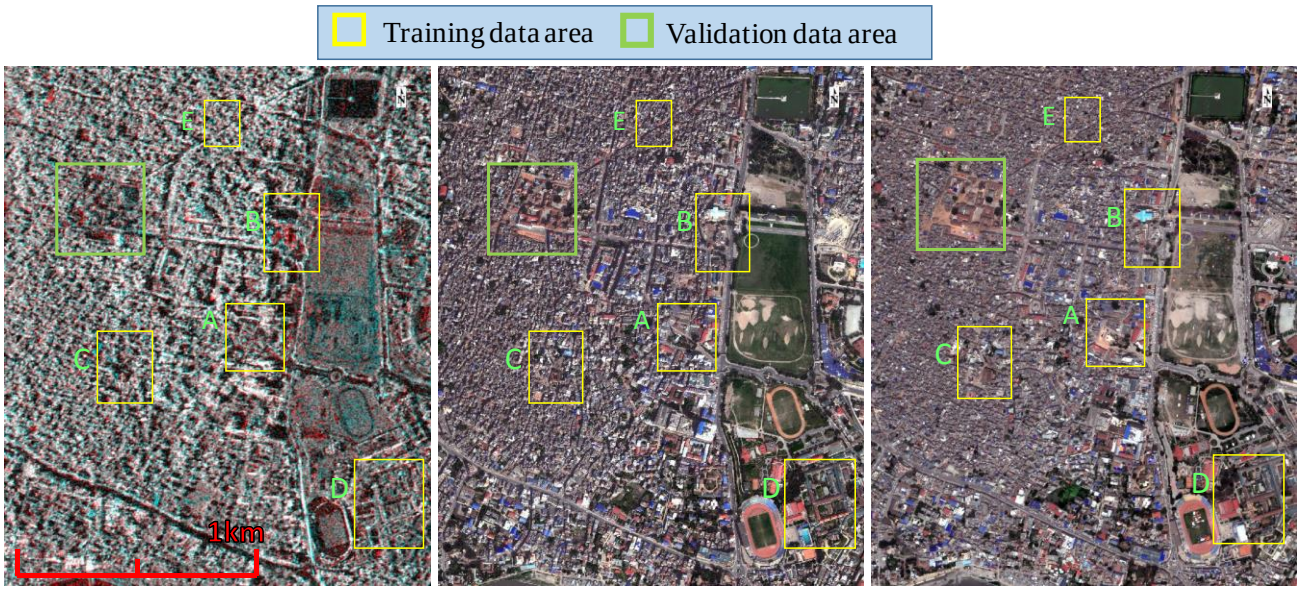

(a) Color composite of TSX (b) Pre-event WV3 (c) Post-event GE1

Figure 2. The study area in the central Kathmandu. (a) the color composite of TSX images with the location of training data and validation data areas, (b) the pre-event WorldView-3, and (c) the post-event GeoEye-1 images.

3. DAMAGE EXTRACTION OF BUILDINGS FROM SAR DATA

The change detection from two-temporal SAR intensity images can be evaluated quantitatively by their difference value, d [dB], and the correlation coefficient, r, by the following equations [13]:

$$d = \bar{Ia}_i - \bar{Ib}_i \tag{1}$$

$$r = \frac{N\sum_{i=1}^{N} Ia_i Ib_i - \sum_{i=1}^{N} Ia_i \sum_{i=1}^{N} Ib_i}{\sqrt{\left(N\sum_{i=1}^{N} {Ia_i}^2 - \left(\sum_{i=1}^{N} Ia_i\right)^2\right)\cdot\left(N\sum_{i=1}^{N} {Ib_i}^2 - \left(\sum_{i=1}^{N} Ib_i\right)^2\right)}} \tag{2}$$

where i is the pixel number, Ia_i and Ib_i are the backscattering coefficient of the second (post-event) and first (pre-event) images, $\bar{Ia}_i$ and $\bar{Ib}_i$ are the corresponding averaged values over the N (= $k \times k$) pixels window surrounding the i-th pixel. The window size, N, may be assigned by considering the spatial resolution of the SAR images and the size of target objects to extract. In this study, the window size of 11x11 pixels (16.5 m x 16.5m) was used.

Figure 3 plots the difference and correlation coefficient images corresponding to the SAR data in Figure 2. Change detection in a period is usually carried out using one of these two indices or using a combined index of the two. For example, Matsuoka and Yamazaki [5, 14] proposed a linear combination of the two indices as an empirical discriminant formula between change and no-change. A similar combined index, z, was also proposed by the current authors [13] as

$$z = \frac{|d|}{Max(|d|)} - cr \tag{3}$$

where $Max(|d|)$ is the maximum absolute value in the difference and c is a weighting constant of the two indices. The correlation coefficient is generally sensitive to subtle changes, and thus it shows a low value even for a small change. On

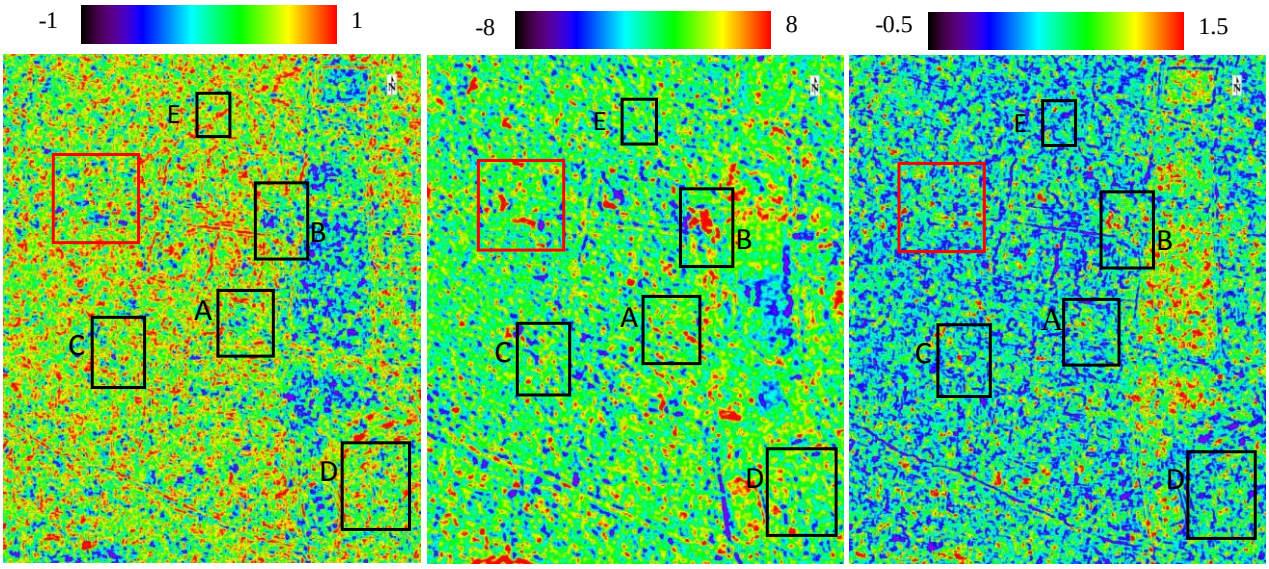

(a) Correlation coefficient, *r* (b) Difference, *d* (c) z-factor

Figure 3. Correlation coefficient (a) and difference (b) of the pre- and post-event backscattering coefficients, and their combined index, z-factor (c), calculated from the TSX images for the study area.

the contrary, the normalized absolute value of the difference is relatively stable. Hence in this study, the weight for difference was set as 2 times of that for correlation (c = 0.5) following the reference [15], and the z-factor for the study area is plotted in Figure 3(c).

Using these parameters, the threshold values for judging collapsed or non-collapsed buildings can be determined by comparing with the optical satellite images and field survey data. A total of 8 collapsed and 28 non-collapsed buildings were selected from the five districts (A-E) shown in Figure 3. Figure 4 shows the enlargement of Figures 2 and 3 for the district A including Dharahara (Bhimsen) tower, which was nine-storey and 61.88-m tall but was completely collapsed due to the mainshock. This tower was rebuilt after the complete collapse due to the 1934 earthquake, but again it was reduced to debris in the 2015 earthquake. From the optical satellite image and aerial videos from a drone [16, 17], the damage levels of the surrounding area was not so severe. Thus, other than Dharahara tower, six large buildings were selected as none-damaged (or at least non-collapsed) ones in Figure 4. Considering the layover of SAR backscatter [7, 10], the location of the roof-prints on the ground level are shown in solid lines while their footprints in broken lines. For Dharahara tower, a red square of 11 x 11 pixels (16.5 m x 16.5 m) was considered as an area to calculate the average value of the three damage indices while for non-damaged buildings, the square areas (within the shifted roof-prints) were used.

It is seen from the figure that low correlation coefficient and negative difference values are seen around the collapsed tower. The z-factor also shows the high possibility of change around the tower. But similar trends showing the high possibility of change are also observed in some other locations in the image. Thus even using high-resolution X-band SAR images, the extraction of severely damaged (or collapsed) buildings form a built-up area is not a very easy task. "Detectability" is highly depending on the spatial resolution of SAR images and built environment, such as the sizes and heights of buildings and the built-up density of the area [9].

Figure 5 shows the enlargement of Figures 2 and 3 for the district B including Tundikhel (large green), which was used as an evacuation site after the earthquake. From the post-event optical satellite image, many tents of the refugees are seen. In this district, three collapsed (or significantly changed) buildings and six non-damaged (or at least non-collapsed) ones were selected as training data. The layover of SAR backscatter was considered to draw the roof-prints of buildings on the ground range. Significant changes were seen in buildings b01, b02 and b03, but the changes in b01 and b02 seem to be non earthquake-related but due to demolition of an old building and construction of new one. The average values of the three damage indices were calculated for the square areas within the shifted roof-prints.

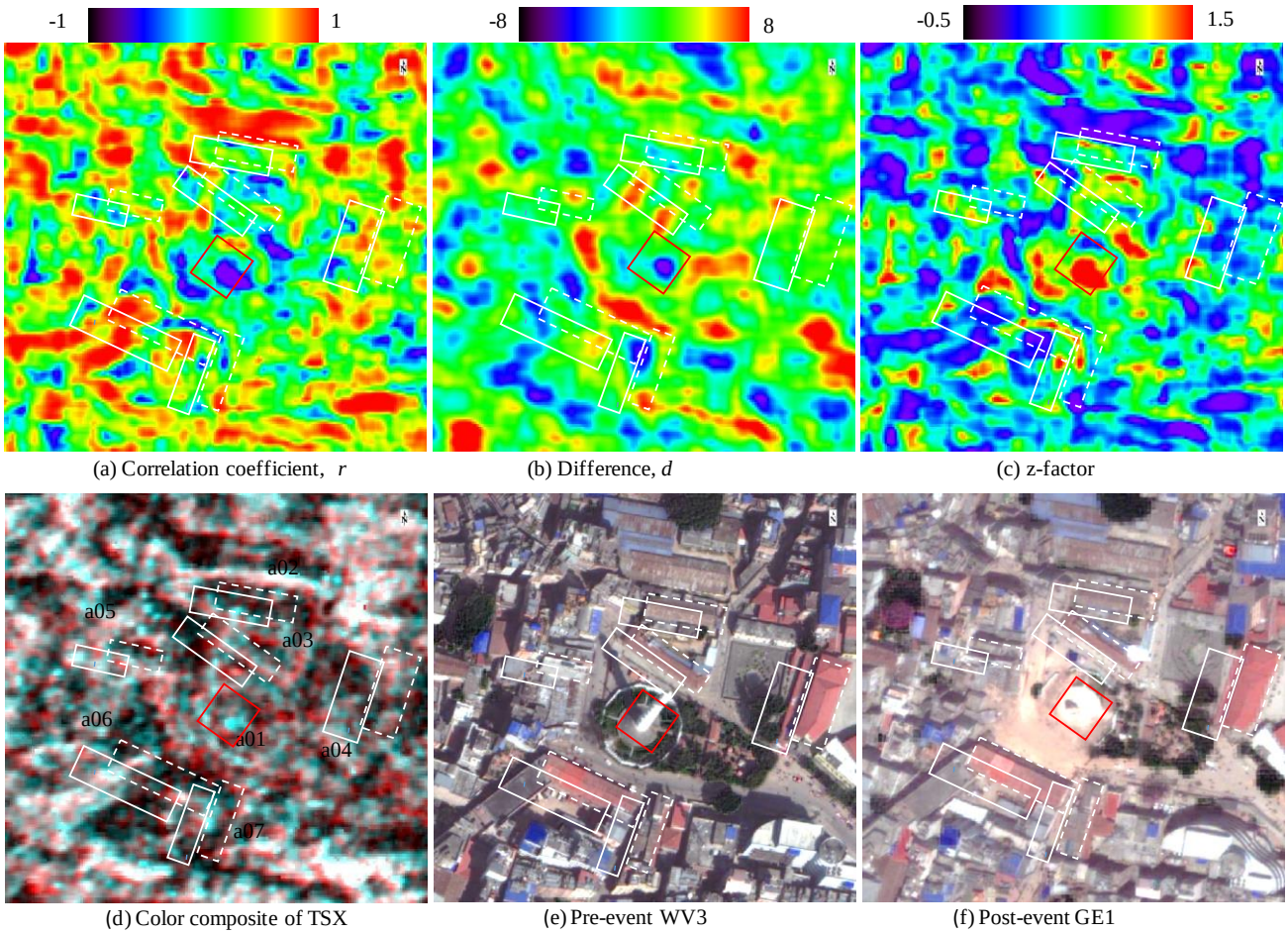

(a) Correlation coefficient, *r* (b) Difference, *d* (c) z-factor

(d) Color composite of TSX (e) Pre-event WV3 (f) Post-event GE1

Figure 4. Correlation coefficient (a) and difference (b) of the pre- and post-event backscattering coefficients, and their combined index, z-factor (c), calculated from the TSX images for the district A including Dharahara Tower. The color composite of the TSX images (d), the pre-event WorldView-3 (e), and the post-event GeoEye-1 images (f) of the same district are shown with the footprints and shifted roof-prints of target buildings (a01-a07).

The similar calculation was also carried out for the districts (C, D, E) in Figure 2. The results of calculation for 36 buildings (8 collapsed/changed and 28 non-collapsed) were plotted in Figure 6 as the relationship between correlation coefficient and difference of two-temporal sigma-naught values. In this plot, the correlation coefficient for the collapsed buildings are less than 0.16 while that for non-collapsed ones are larger than 0.16. Hence this threshold value can be used to extract collapsed buildings if the footprints of buildings are available from GIS data or from pre-event optical images. The difference values for non-collapsed buildings were mostly within plus minus 2 dB while for the collapsed buildings, the absolute values of the difference were mostly larger than 2 dB. This tendency of the correlation coefficient and difference of TerraSAR-X for collapsed buildings was similar to our study on the Nepal earthquake using PALSAR-2's L-band data [17].

The difference of backscatter (the sigma naught value) is reduced because a double-bounce component from the building wall becomes small after the collapse or significant damage [5]. But in some situations, collapsed buildings may return stronger backscatter than intact flat-roofs do. Debris surrounding collapsed buildings also gives stronger backscatter than bare ground does. Considering these situations, the current authors introduced the z-factor, which can cope with both increased and decreased backscatter from severely damaged or washed-away buildings [15]. The relationship between the correlation coefficient and z-factor of the two-temporal sigma-naught values is shown in Figure 7. In this plot, the z-factor for the collapsed buildings are larger than 0.12 while that for non-collapsed ones are less than 0.12 except for one

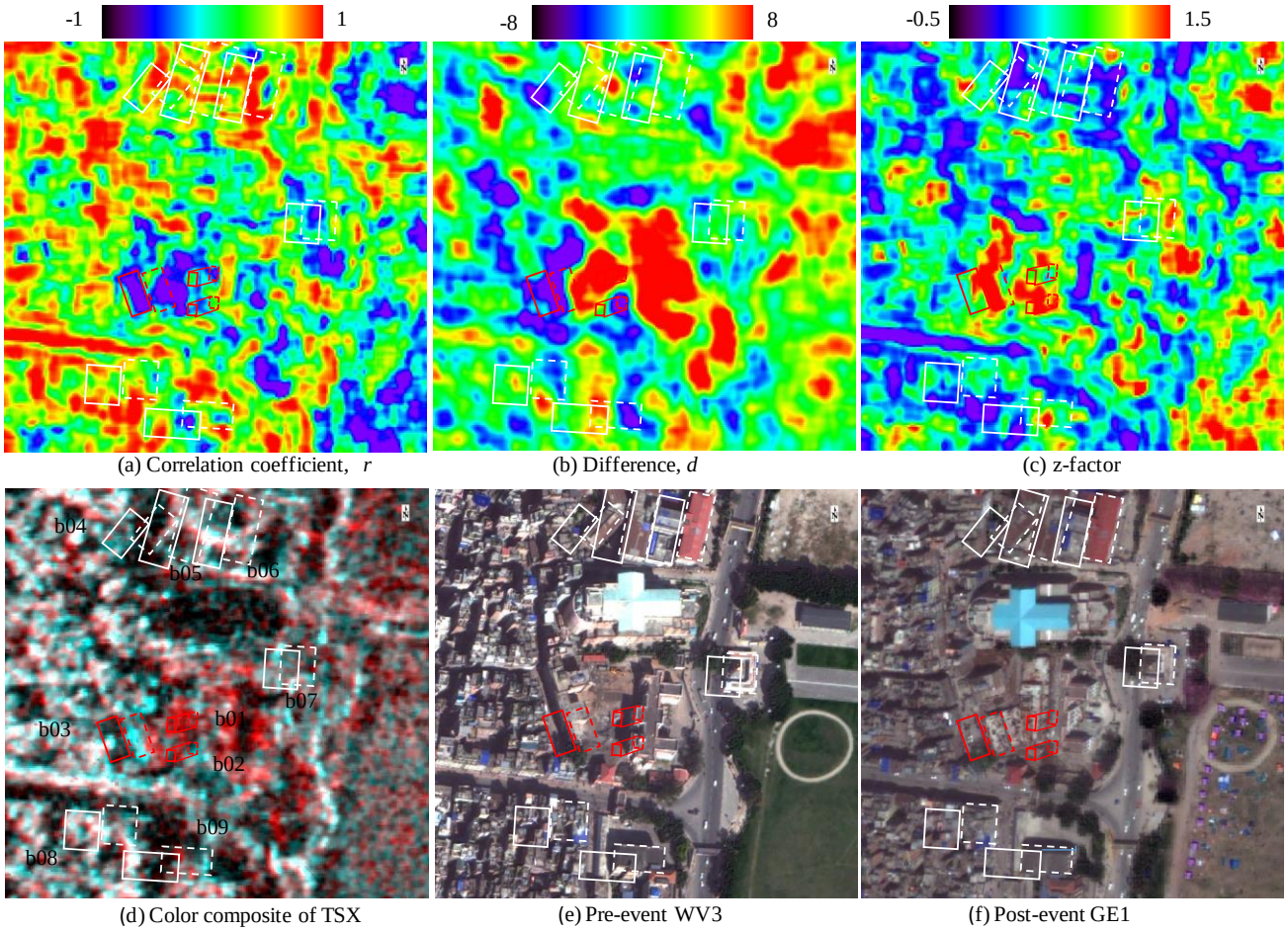

(a) Correlation coefficient, *r* (b) Difference, *d* (c) z-factor

(d) Color composite of TSX (e) Pre-event WV3 (f) Post-event GE1

Figure 5. Correlation coefficient (a) and difference (b) of the pre- and post-event backscattering coefficients, and their combined index, z-factor (c), calculated from the TSX images for the district B including Tundikhel. The color composite of the TSX images (d), the pre-event WorldView-3 (e), and the post-event GeoEye-1 images (f) of the same district are shown with the footprints and shifted roof-prints of target buildings (b01-b09).

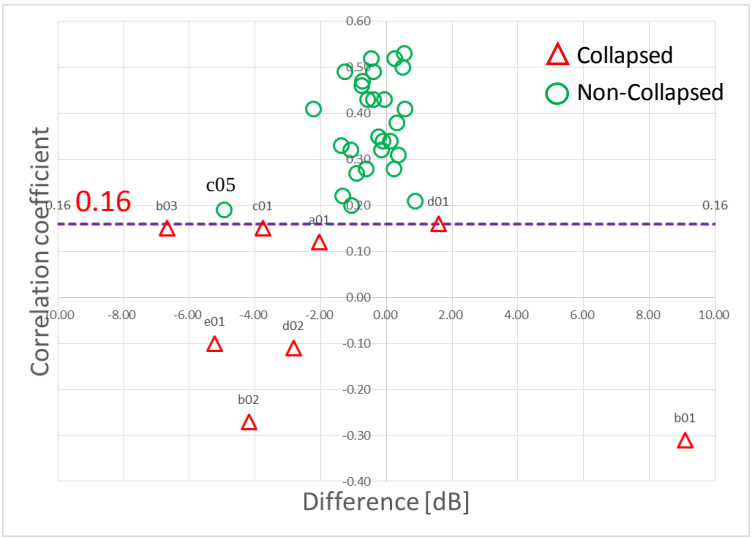

Figure 6. Relationship between correlation coefficient and difference of two-temporal sigma-naught values for 36 buildings

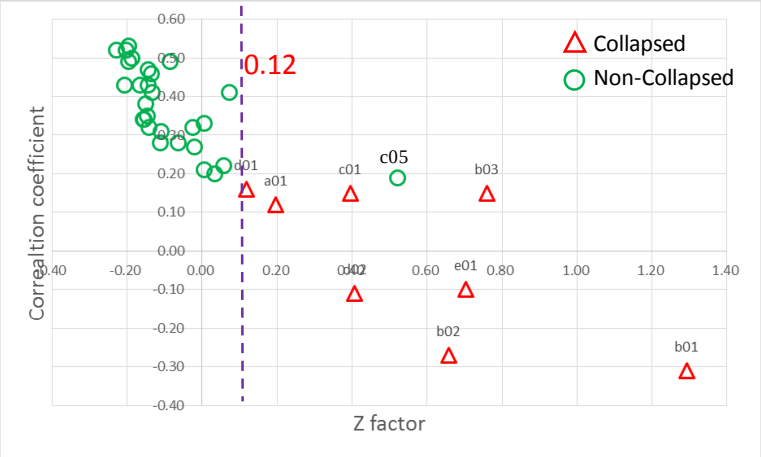

Figure 7. Relationship between correlation coefficient and z-factor of two-temporal sigma-naught values for 36 buildings

building (c05). This building is the only outlier in Figure 6 also. Although the building looks like no damage from the vertical optical images, there is a possibility of some changes, especially in its layover area because of the reduced backscattering coefficient. Since the z-factor represents both the difference and correlation coefficient, it was affected by the change in the difference also. On the contrary, this outlier did not affect the correlation coefficient and hence, its threshold was perfect for the training data used in this study.

4. VALIDATION OF THE EXTRACTION METHOD OF COLLAPSED BUILDINGS

The threshold values to extract individual collapsed buildings were tested for the area that was not used to determine these values. "Durbar Square" means plazas and areas opposite the old royal palaces in Nepal. Three Durbar Squares, Kathmandu, Patan, and Bhaktapur, are located in the Kathmandu valley, and all the three have been designated as the world heritage site out of seven monument zones in the Kathmandu valley. Since Hanuman Dhoka (Kathmandu) Durbar Square is the most famous tourist site in Nepal, mass media broadcasted the damage situation of this site frequently. A video taken from UAV [18] showed the damage situation of the Durbar Square quite well, as shown in a snapshot in Figure 8 (a). Using the video footage, we developed a 3D model of this area with the aid of Agisoft's *PhotoScan* software [19]. Another reason of selecting this site for validation is that a damage situation map of the monuments in the square, shown in Figure 8 (b), was found in the field survey trip in September 2015 by the third author. This map was made by the local government, and three damage levels, *totally damaged*, *partially damaged*, and *safe monument*, were assigned.

The close-up of this area from the pre- and post-event high-resolution optical images is also shown in Figure 8 (c) and (d). From these vertical optical images, damage situations of some "totally damaged" buildings are not easy to recognize. Using also the aerial video footage and the photos taken from the ground, the "totally damaged" buildings were re-classified into two levels, collapsed (5 buildings, red) and major damage (11 buildings, yellow), as shown in Figure 8 (c) and 8(d). From the structures in the palace and buildings facing to the square, 22 minor-damaged buildings were also assigned as in green frames. A total of 38 buildings were used from the validation of the damage extraction method.

Figure 9 shows the distributions of the correlation coefficient (r) and difference (d) of the pre- and post-event backscattering coefficients, and their combined index (z), together with their color composite for Kathmandu Durbar Square area. From the figure, the three damage indices were averaged within the shifted roof-print of each building and the result was plotted in Figure 10 as the relationship between the correlation coefficient and difference of the two-temporal backscattering coefficients for the 38 buildings in this site. From the plot, all the 5 collapsed buildings have the correlation coefficient (r) less than the threshold value (0.16), and all the 22 minor-damaged buildings have the value larger than the threshold. But for 11 major-damaged buildings, 5 buildings have the value satisfying the damage criteria while 6 others have the value larger than the threshold.

(a) Drone video footage of Durbar Square area

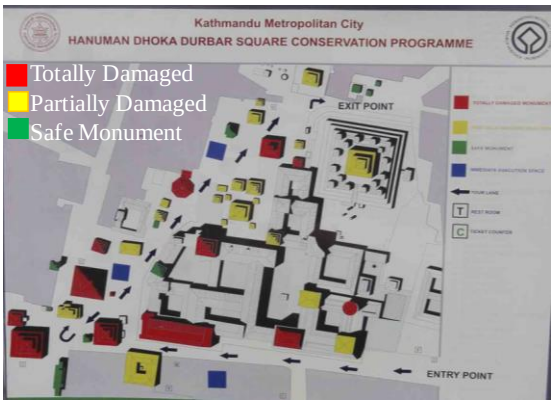

(b) Damage map of monuments in Durbar Square

(c) Pre-event WV3 image with reclassified damage level

(d) Post-event GE1 image with reclassified damage level

Figure 8. Truth data of building damage in Kathmandu Durbar Square. A snapshot of drone video footage (a), damage map of monuments by Kathmandu city government (b), the pre-event WorldView-3 (c), and the post-event GeoEye-1 images (d) of the Durbar Square with reclassified building damage level.

Based on these observations, the confusion matrix was made as shown in Table 1. In the table, major-damaged buildings in the truth data were considered as the same category "collapsed buildings". In this condition, 6 major-damaged buildings were categorized as "non-collapsed" from the TerraSAR-X's image analysis, indicating false-negative (or omission error) in the collapsed building extraction. But for "collapsed" and "minor damage" categories of the truth data, they were all correctly identified.

In summary, satellite SAR intensity data are quite useful in extracting collapsed large buildings, but as the damage level gets smaller, damage extraction becomes difficult. Damage extraction goes much more difficult for small buildings and for those in densely built-up urban areas. These observations agree well with our previous experiences using high-resolution SAR data [9, 20]. However, more case studies with field validation data are necessary to enhance damage extraction methods using multi-temporal SAR intensity data.

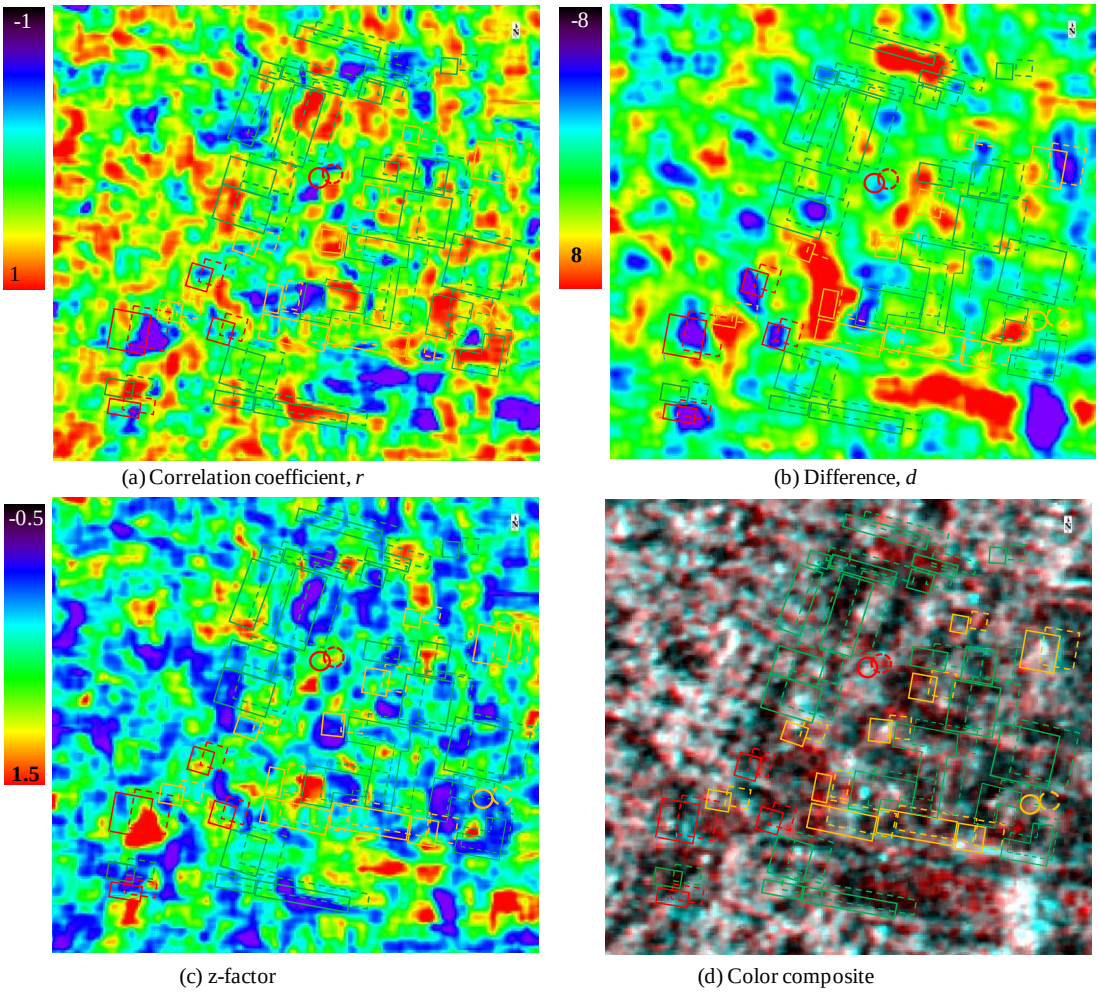

(a) Correlation coefficient, *r* (b) Difference, *d*

(c) z-factor (d) Color composite

Figure 9. Correlation coefficient (a) and difference (b) of the pre- and post-event backscattering coefficients, and their combined index, z-factor (c), calculated from the TSX images, and their color composite (d) for the area including Kathmandu Durbar Square. The color of the building frame indicates a reclassified building damage level.

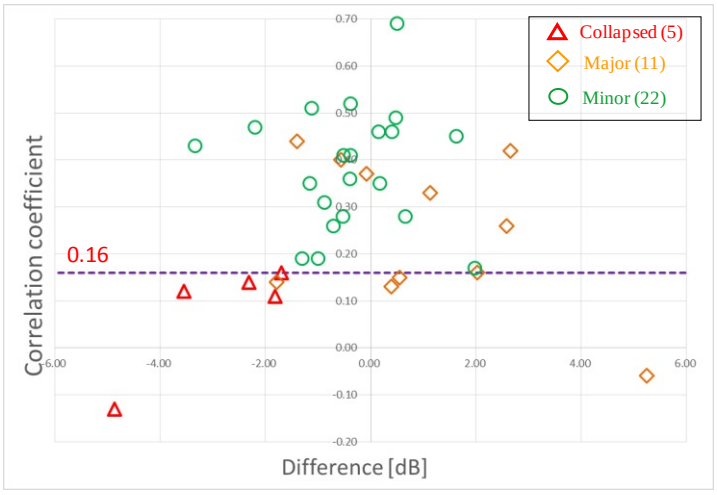

Figure 10. Relationship between the correlation coefficient and difference for 38 buildings in Kathmandu Durbar Square.

Table1. Confusion matrix for 38 buildings in Kathmandu Durbar Square based on the threshold value (r=0.16) of the correlation coefficient dividing collapsed and non-collapsed buildings

		Truth Data				
		Collapsed	Major Damage	Minor Damage	Total	User Accuracy (%)
Extraction by TerraSAR-X	Collapsed	**5**	**5**	0	10	100.0
	Non-Collapsed	0	6	**22**	27	81.5
	Total	5	11	22	**38**	
	Producer Accuracy (%)	100.0	45.5	100.0		Overall Accuracy (%) 84.2

5. CONCLUSION

Recently satellite SAR data became one of the useful tools for detecting and monitoring affected areas due to natural disasters because SAR can capture the earth surface's condition both at daytime and nighttime and under cloud-cover situation. In this study, multi-temporal high-resolution TerraSAR-X images were used for damage inspection of the Kathmandu area, which was severely affected by the Mw7.8 25 April 2015 Gorkha, Nepal earthquake. The SAR images obtained before and after the earthquake were utilized for calculating the difference and correlation coefficient of the backscattering coefficient values. The affected areas were characterized by low values of the correlation coefficient, representing the changes that occurred in the period. Pre- and post-event high-resolution optical satellite images, aerial video footage, and field survey photos were employed as ground truth data to examine our analysis results. A threshold value of the correlation coefficient was determined for training areas in the central Kathmandu. Then this threshold was applied to the structures in Kathmandu Durbar Square and the result was compared with the damage map produced by the local government. Although it was difficult to identify the damage levels for individual buildings, large collapsed buildings could be well extracted from the SAR images. Thus high-resolution SAR data can provide early stage information on the damage of built environments.

ACKNOWLEDGEMENT

The TerraSAR-X data are the property of the German Aerospace Center (DLR) and Inforterra GmbH and were made available by the PASCO Corporation through the joint research between PASCO Co. and Chiba University. The field survey was conducted as a part of J-RAPID project "Reevaluation of seismic vulnerability on historic structures based on damage investigation of the 2015 Nepal earthquake and of retrofitting methods", headed by Prof. Junji Kiyono of Kyoto University. This study was financially supported by a Grant-in-Aid for Scientific Research (Project numbers: 15K16305, 24241059) of the Japan Society for the Promotion of Science (JSPS).

REFERENCES

[1] United States Geological Survey (USGS), "M7.8 - 36km E of Khudi, Nepal –Earthquake Hazard Program," http://earthquake.usgs.gov/earthquakes/eventpage/us20002926#general_region (15 February 2016).
[2] National Society for Earthquake Technology-Nepal, "Gorkha Earthquake - Nepal rattled by 7.6 Magnitude Earthquake," http://www.nset.org.np/eq2015/ (15 February 2016).
[3] Stramondo S., Cinti F.R., Dragoni M., Salvi S. and Santini S., "The August 17, 1999 Izmit, Turkey, earthquake: Slip distribution from dislocation modeling of DInSAR and surface offset," Annals of Geophysics, 45(3/4), 527-536 (2002).

[4] Yonezawa, C., and Takeuchi, S., "Decorrelation of SAR data by urban damages caused by the 1995 Hyogoken-Nanbu Earthquake," International Journal of Remote Sensing, 22(8), 1585–1600 (2001).
[5] Matsuoka, M., and Yamazaki, F., "Use of satellite SAR intensity imagery for detecting building areas damaged due to earthquakes," Earthquake Spectra, 20(3), 975-994 (2004).
[6] Matsuoka, M. and Yamazaki, F., "Building damage mapping of the 2003 Bam, Iran, Earthquake using Envisat/ASAR intensity imagery, " Earthquake Spectra, 21, S285–S294 (2005).
[7] Brunner, D., Lemoine, G. and Bruzzone L., "Earthquake damage assessment of buildings using VHR optical and SAR imagery, " IEEE Transactions on Geoscience and Remote Sensing, 48(5), 2403–2420 (2010).
[8] Wang, T.L. and Jin Y.Q., "Postearthquake building damage assessment using multi-mutual information from pre-event optical image and postevent SAR image," IEEE Geoscience and Remote Sensing Letters, 9(3), 452–456 (2012).
[9] Uprety, P., and Yamazaki, F., and Dell' Acqua, F., "Damage detection using high-resolution SAR imagery in the 2009 L'Aquila, Italy, Earthquake," Earthquake Spectra, 29(4), 1521-1535 (2013).
[10] Yamazaki, F. Iwasaki, Y., Liu, W. Nonaka, T. and Sasagawa, T, "Detection of damage to building side-walls in the 2011 Tohoku, Japan earthquake using high-resolution TerraSAR-X images," Proc. SPIE 8892, Image and Signal Processing for Remote Sensing XIX, 889212; doi:10.1117/12.2029465 (2013).
[11] Japan Society of Civil Engineers, "Quick reconnaissance report on the April 25, 2015 Gorkha, Nepal earthquake," http://committees.jsce.or.jp/eec2/node/61 (15 February 2016)
[12] PASCO Co., "TerraSAR-X Basic Image Products," http://www.pasco.co.jp/eng/products/terrasarx/ (15 February 2016).
[13] Yamazaki, F. and Liu, W., "Urban change monitoring: multi-temporal SAR images," Encyclopedia of Earthquake Engineering, DOI 10.1007/978-3-642-36197-5_227-1, Springer-Verlag Berlin Heidelberg (2014).
[14] Matsuoka, M. and Yamazaki, F., "Comparative analysis for detecting areas with building damage from several destructive earthquakes using satellite synthetic aperture radar images," Journal of Applied Remote Sensing, SPIE, Vol.4, 041867, doi:10.1117/1.3525581 (2010).
[15] Liu, W., Yamazaki, F., Gokon, H., and Koshimura, S., "Extraction of tsunami-flooded areas and damaged buildings in the 2011 Tohoku-Oki Earthquake from TerraSAR-X intensity images," Earthquake Spectra, 29(S1), S183-S200 (2013).
[16] CNN, "Drone footage over Kathmandu shows quake damage," https://www.youtube.com/watch?v=KtXv7PLnR4o (15 February 2016).
[17] Bahri, R., Liu, W. and Yamazaki, F., "Damage assessment of urban areas due to the 2015 Nepal earthquake using PALSAR-2 imagery," Proc. 36th Asian Conference on Remote Sensing, Manila, Philippines, 10p (2015).
[18] Storyful News, " Drone Footage Captures Aftermath of Nepal Earthquake," https://www.youtube.com/watch?v=N52LX1GZYWs (27 February 2016).
[19] Yamazaki, F., Matsuda, T., Denda, S. and Liu, W., "Construction of 3D models of buildings damaged by earthquakes using UAV aerial images," Proceedings of the Ninth Pacific Conference on Earthquake Engineering, Sydney, Australia, Paper No. 204, 8p (2014).
[20] Uprety, P. and Yamazaki, F., "Detection of building damage in the 2010 Haiti earthquake using high-resolution SAR intensity images, Journal of Japan Association for Earthquake Engineering, 12(6), 21-35 (2012).